

RESEARCH ARTICLE

10.1002/2015GC005744

Experimental mixtures of superparamagnetic and single-domain magnetite with respect to Day-Dunlop plots

Monika Kumari¹, Ann M. Hirt¹, Rene Uebe^{2,3}, Dirk Schüler^{2,3}, Éva Tompa⁴, Mihály Pósfai⁴, Wolfram Lorenz⁵, Fredrik Ahrentorp⁶, Christian Jonasson⁶, and Christer Johansson⁶

Key Points:

- SP-SD mixtures of magnetite may not follow theoretical predictions
- Size, shape, and/or measurement time interaction play a role in SD-SP mixtures
- SP-SP clustering can cause the observed discrepancy

Supporting Information:

- Supporting Information S1

Correspondence to:

A. M. Hirt,
ann.hirt@erdw.ethz.ch

Citation:

Kumari, M., A. M. Hirt, R. Uebe, D. Schüler, É. Tompa, M. Pósfai, W. Lorenz, F. Ahrentorp, C. Jonasson, and C. Johansson (2015), Experimental mixtures of superparamagnetic and single-domain magnetite with respect to Day-Dunlop plots, *Geochem. Geophys. Geosyst.*, 16, 1739–1752, doi:10.1002/2015GC005744.

Received 21 JAN 2015

Accepted 15 MAY 2015

Accepted article online 21 MAY 2015

Published online 12 JUN 2015

¹Department of Earth Sciences, Institute of Geophysics, ETH-Zurich, Zurich, Switzerland, ²Department Biologie I, Ludwig Maximilian University of Munich, Munich, Germany, ³Now at Department of Microbiology, University of Bayreuth, Bayreuth, Germany, ⁴Department of Earth and Environmental Sciences, University of Pannonia, Veszprém, Hungary, ⁵Department of Physics, Institute of Solid State Physics, ETH Hönggerberg, Zurich, Switzerland, ⁶Acreeo Swedish ICT AB, Gothenburg, Sweden

Abstract Day-Dunlop plots are widely used in paleomagnetic and environmental studies as a tool to determine the magnetic domain state of magnetite, i.e., superparamagnetic (SP), stable single-domain (SD), pseudosingle-domain (PSD), multidomain (MD), and their mixtures. The few experimental studies that have examined hysteresis properties of SD-SP mixtures of magnetite found that the ratios of saturation remanent magnetization to saturation magnetization and the coercivity of remanence to coercivity are low, when compared to expected theoretical mixing trends based on Langevin theory. This study reexamines Day-Dunlop plots using experimentally controlled mixtures of SD and SP magnetite grains. End-members include magnetotactic bacteria (MSR-1) as the SD source, and a commercial ferrofluid or magnetotactic bacteria ($\Delta A12$) as the SP source. Each SP-component was added incrementally to a SD sample. Experimental results from these mixing series show that the magnetization and coercivity ratios are lower than the theoretical prediction for bulk SP magnetic size. Although steric repulsion was present between the particles, we cannot rule out interaction in the ferrofluid for higher concentrations. The SP bacteria are noninteracting as the magnetite was enclosed by an organic bilipid membrane. Our results demonstrate that the magnetization and coercivity ratios of SD-SP mixtures can lie in the PSD range, and that an unambiguous interpretation of particle size can only be made with information about the magnetic properties of the end-members.

1. Introduction

The grain size of ferromagnetic (s.l.) minerals plays an important role in paleomagnetism when one needs to understand the stability of magnetization in rocks and sediments. It is also of great interest in environmental magnetic studies, where grain size can reflect provenance, and will be influenced by geochemical processes. Many methods have been proposed to obtain the grain size distribution of magnetic minerals. These include microscopic methods, e.g., transmission electron microscopy, scanning electron microscopy, and methods that exploit magnetic properties that are sensitive to grain size [e.g., *Carter-Stiglitz et al.*, 2001; *Day et al.*, 1977; *Dunlop*, 2002a, 2002b; *Heslop and Roberts*, 2012; *Jackson et al.*, 1990; *Kumari et al.*, 2014; *Tauxe et al.*, 1996; *von Dobeneck*, 1996]. In practice, the Day plot has established itself as one of the most common tools to define domain states and grain sizes for magnetite and more recently for greigite [*Roberts et al.*, 2011].

The Day plot combines theoretically derived parameters with empirical results, which were obtained from titanomagnetite with varying grain size fractions. It represents the ratio of remanent coercivity (H_{CR}) to coercivity (H_C) plotted as a function of the ratio of remanent magnetization (M_{RS}) to saturation magnetization (M_S). The Day plot is categorized into three sections that indicate single-domain (SD), pseudosingle-domain (PSD), or multidomain (MD) behavior. Later *Dunlop* [2002a] modified the original Day plot by suggesting new boundary limits for the three domain states. By assuming noninteracting magnetite SD grains, the boundaries in domain state were set at $M_{RS}/M_S \geq 0.5$ and $1 \leq H_{CR}/H_C \leq 2$; the limits are $0.02 \leq M_{RS}/M_S \leq 0.5$ and $2 \leq H_{CR}/H_C \leq 5$ for PSD grains; and $M_{RS}/M_S \leq 0.02$ and $H_{CR}/H_C \geq 5$ for MD grains. He also incorporated mixing lines for grain size distributions that include SD-PSD and SD-MD mixtures, and calculated a range of mixing lines for superparamagnetic (SP) and SD mixtures depending upon the size of the SP grains [*Dunlop*, 2002a]. These theoretical curves for SD-SP mixtures are derived under the following approximations: (a) the

two end-members consist of stoichiometrically pure magnetite, whereby the ratio of magnetization shows linear additivity with respect to the end-members; (b) the SD magnetite consists of identical, uniaxial, and noninteracting grains, in which induced magnetization is linear between $-M_{RS}$ and H_C and backfield isothermal remanent magnetization is linear between M_{RS} and $-H_{CR}$; and (c) the SP magnetite is also made up of identical and noninteracting grains whose magnetization curve is governed by a Langevin function that is linear to the applied magnetic field, H , and saturates at lower values of H .

A large number of paleomagnetic studies that employ a Day-Dunlop plot find often that the samples fall into the PSD size range [e.g., Cinku *et al.*, 2013; Di Chiara *et al.*, 2014; Guzmán *et al.*, 2011; Hao *et al.*, 2012; Kapper *et al.*, 2014; Li *et al.*, 2014; Stanton *et al.*, 2011; Tianshui *et al.*, 2012]. One possible reason could be that the samples consist of mixtures of grain sizes. Few studies have investigated how mixtures of magnetite with known particle sizes match with predictions of SD-MD, SD-PSD, and SD-SP mixtures on a Day-Dunlop plot [Dunlop, 2002a, 2002b; Dunlop and Carter-Stiglitz, 2006; Lanci and Kent, 2003; Lees, 1997]. Dunlop and Carter-Stiglitz [2006] evaluated one mixture that consisted of SD magnetite obtained from magnetotactic bacteria for the SD end-member and ferrofluid with an average magnetite diameter of 10 nm for the SP end-member. Their SD-SP mixing curve falls below and/or to the left of the expected theoretical mixing trend for 10 nm SP particles. The authors attributed this difference to interactions, which will affect the effective particle volume if aggregation occurs, thereby reducing the initial SP susceptibility. The authors did not, however, experimentally determine if particle interaction occurs.

This study reexamines Day-Dunlop plots for SD-SP mixtures of well-characterized end-members. The first case repeats the experiment of Dunlop and Carter-Stiglitz [2006] with a mixture of bacterial SD magnetite and ferrofluid. The second case considers a mixture of SD and SP magnetite, which are both of bacterial origin. The results are compared to the earlier study of Dunlop and Carter-Stiglitz [2006], and sources of discrepancies with theoretical curves are discussed in relationship to the applicability of the plot in predicting the percentage of SP particles and their sizes in a SD-SP mixture.

2. Methods and Samples

2.1. Methods

2.1.1. Transmission Electron Microscopy

Transmission electron microscopy (TEM) analyses of the end-members, i.e., SD-bacteria, SP-ferrofluid, and SP-bacteria, were made at three different places. The SD-bacteria were imaged at the Scientific Center for Optical and Electron Microscopy (ScopeM) at ETH-Zurich using a FEI Morgagni 268, operated at 100 kV. The ferrofluid was analyzed at the Research Institute for Technical Physics and Materials Sciences in Budapest, Hungary using a JEOL 3010 microscope, operated at 300 kV, and TEM micrographs of SP-bacteria were obtained at LMU Munich using a FEI Tecnai F20 transmission electron microscope at an accelerating voltage of 200 kV.

2.1.2. Magnetic Measurements

Induced magnetization, acquisition of an isothermal remanent magnetization in backfield (DC-IRM) and first-order reversal curves (FORC) [Carvallo *et al.*, 2006; Muxworthy *et al.*, 2004; Pike *et al.*, 1999, 2001; Roberts *et al.*, 2000] were performed on a vibrating sample magnetometer (VSM, model 3900) from Princeton Measurement Corporation (PCM). Hysteresis loops were measured between ± 1 T with a 100 ms averaging time, using a varying field increment: a 0.5 mT field increment was used between ± 20 mT, 1 mT increment in the range $|20|$ – $|100|$ mT, and 10 mT increment in higher fields. The DC-IRM curve was acquired at room temperature by saturating SD-bacteria in a field of +1 T, and then remagnetizing the sample in the opposite direction, to obtain H_{CR} . Measurements were made with a 0.01 T increment and 100 ms averaging time. Because it was not possible to normalize the magnetic moment by the Fe content, we give results in terms of the total magnetic moment.

The FORC protocol for the SD-bacteria plus SP-ferrofluid series consists of 180 curves with a field increment of 1.3 mT. However, a set of 240 curves for the mixtures of SD-bacteria and SP-bacteria were made with a field increment of 0.61 mT to increase the signal-to-noise ratio, due to the weak magnetic properties of the samples. FORC data were processed using the M. Winklhofer MATLAB code [Winklhofer and Zimanyi, 2006] with smoothing factor, $SF = 2$, unless otherwise given. The first point artifact is removed. In a FORC diagram, the horizontal axis denotes the distribution of coercive field (H_A), which is sensitive to composition and grain size of the ferromagnetic (s.l.) phases, while the vertical axis (H_U) provides information on magnetic

interaction between the particles. The full width at half maxima $H_{A1/2}$ and $H_{U1/2}$ were used to characterize interactions in these samples.

Frequency-dependent susceptibility (AC susceptibility) in a large frequency range at room temperature was measured with two AC susceptometer instruments, the DynoMag system from Acreo Swedish ICT AB (frequency range 1 Hz–500 kHz) and a prototype high-frequency (HF) AC susceptometer (frequency range 20 kHz–10 MHz) at Acreo Swedish ICT AB. Measurements were all carried out at 298 K in the frequency range from 1 Hz to 10 MHz [Ferguson *et al.*, 2013]. The field amplitude is 0.5 mT for the DynoMag system and 30 μ T for the HF system. Both AC susceptometer systems are calibrated against a Dy_2O_3 sample (paramagnetic substance) over the entire frequency range with respect to signal response amplitude and phase. The AC susceptibility is given in volume susceptibility (SI units). The sample volume is used to normalize the measured AC magnetic moments. Since the samples are liquids, it is easier to use the sample volume and report the volume susceptibility. It is simple to convert the volume susceptibility to mass susceptibility by dividing the volume susceptibility by the density of the samples (close to 1000 kg/m³, carrier liquid is water) to get the mass susceptibility in m³/kg. The sample volumes are 0.2 mL.

An AC susceptibility model is based on the Debye expression, which is integrated over a size distribution (lognormal function) for the Brownian relaxation part and a Cole-Cole expression for the Néel relaxation [Öisjöen *et al.*, 2010]. This AC susceptibility model was fitted to the AC susceptometry data to determine the particle size distribution and type of magnetic relaxation (Brownian and Néel relaxation or a combination) of the magnetic nanoparticle systems [Öisjöen *et al.*, 2010]. Néel relaxation is the internal relaxation process in single-domain nanocrystals and is dependent for instance on the energy barrier, i.e., the product of the magnetic anisotropy and the volume of the single-domain nanocrystal. Brownian relaxation is the stochastic relaxation process, which occurs when particles are placed in a liquid; it is dependent on the viscosity of the liquid and the hydrodynamic volume of the particle [Krishnan, 2010]. The different relaxation processes for a nanoparticle system in a carrier liquid can be determined by studying in which frequency range the relaxation features occurs, i.e., changes in the in-phase and out-of-phase components of the AC susceptibility. Generally, for magnetic nanoparticles dispersed in a carrier liquid that exhibit Brownian relaxation, the relaxation is seen below 100 kHz while the Néel relaxation is observed above 100 kHz [Krishnan, 2010]. Frequency-dependent susceptibility was also measured as a function of temperature on a Quantum Design Physical Properties Measurement System (PPMS-14T) at the Institute of Solid State Physics, ETH Zürich in seven frequencies between 10 Hz and 10 kHz, using a 5 K measurement interval between 5 and 300 K.

In order to characterize magnetostatic interaction in SD-bacteria, IRM acquisition and alternating field (AF) demagnetization curves were performed using a 2G Enterprises SQUID rock magnetometer (Model 755), kept inside a magnetically shielded room. The sample was first subjected to AF demagnetization along all three axes and subsequently given a magnetization in a known direction, using an ASC Impulse Magnetizer (Model IM-10–30). The magnetization acquired was then measured as a function of applied magnetic field strength. Finally, the sample was stepwise demagnetized in the direction in which the remanence was acquired.

2.2. Sample Description

2.2.1. End-Members

The end-members that were used for the two SD-SP mixing series consist of: (a) *Magnetospirillum gryphiswaldense* strain MSR-1, as the source of SD-magnetite for both series; (b) ferrofluid, FluidMAG-D (Article number: 4101-1; 4101-5), which was purchased from Chemicell GmbH with a mean hydrodynamic diameter of 45 nm and magnetite nanocrystal size of 10 nm as one SP end-member; and (c) *Magnetospirillum gryphiswaldense* strain Δ A12, whose mean particle size is reported to be 18.4 ± 6.0 nm [Lohsse *et al.*, 2011], as the SP end-member in the second series. Note that the minor variations in cultivation conditions and growth phases can lead to smaller or larger average size. The individual magnetite nanoparticles within MSR-1 and Δ A12 bacterium are surrounded by a lipid bilayer that protects the magnetite from oxidation and clustering. The synthetic SP particles were coated with starch that provides steric repulsion between the particles to prevent oxidation and aggregation.

2.2.2. SD-SP Mixing Series

Two different samples were prepared from the MSR-1 sample. Both were dried in a small capillary tube and are referred to as SD-bacteria. They served as the initial material for both mixing series; (a) SD-bacteria plus SP-ferrofluid, and (b) SD-bacteria plus SP-bacteria. A small amount of the SP sample was added

incrementally to the fixed amount of SD-bacteria. Measurements were performed on dried and immobilized samples after each addition.

3. Results

3.1. TEM Results

TEM analysis was done for the end-members. The SD-bacteria contain chains of euhedral magnetite crystals with an average size of 35 ± 10 nm, but with a distribution in particle sizes between ~ 10 and 60 nm (Figure 1a). The magnetite particles from ferrofluid formed a continuous film on the TEM grid and were embedded in an amorphous material that resulted in a poor TEM image contrast. This made it difficult to measure the particle size distribution due to aggregation. A mean iron-core size was determined from 24 individual particles and gave an average size of 6 nm (Figure 1b). The diameter of particle aggregates, however, is approximately 10–12 nm. The $\Delta A12$ bacteria contain isolated magnetite crystals that are dispersed and have an average size of 14 ± 6 nm (Figure 1c). This size falls within the range reported for the $\Delta A12$ strain by *Lohsse et al.* [2011]; however, there are also a few larger magnetosomes of single-domain size in individual bacterium cells.

3.2. Magnetic Results

3.2.1. End-Member Magnetic Properties

Figure 2 shows the hysteresis loops, IRM acquisition, and FORC diagram of the SD-bacteria at room temperature. The hysteresis loops are open with $H_C = 11.3$ mT (Figure 2a), and the dc-IRM curve is saturated at fields of approximately 100 mT (Figure 2b). M_{RS}/M_S and H_{CR}/H_C from the hysteresis loops are 0.45 and 1.3, respectively. These values are consistent with those reported for magnetosomes in intact chains [*Denham et al.*, 1980; *Fischer et al.*, 2008; *Moskowitz et al.*, 1993]. They deviate slightly, however, from the ideal values for noninteracting SD magnetite with shape anisotropy reported by *Day et al.* [1977], i.e., $M_{RS}/M_S = 0.5$ and $H_{CR}/H_C = 1.5$. This is attributed to the presence of a minor contribution from nascent SP particles at the ends of the chains [*Pan et al.*, 2005]. The FORC diagram shows a characteristic elongated coercivity distribution with a peak around 13.5 mT and $H_{U1/2} = 3.5$ mT (Figure 2c). The low value of $H_{U1/2}$ indicates negligible or no interaction among the individual magnetite nanoparticles. The FORC diagram also displays a pronounced negative region in the lower H_U region close to $H_A = 0$ indicative of noninteracting SD grains [*Newell*, 2005]. The reversible and irreversible components for the SD-bacteria show that some particles are relaxing over the measurement scale of 100 ms, in which the fraction of SP particles is $\approx 16\%$ of the total magnetic response [*Kumari et al.*, 2014].

The hysteresis loops for both SP samples are closed, thus having a negligible magnetization ratio (Figure 2d). The magnetic moment of the SP bacteria is very weak, which accounts for the noisier measurements. Their FORC distributions are centered at the origin of the diagram with a positive shift along the axis of the interaction field (Figures 2e and 2f).

3.2.2. AC Susceptibility Versus Frequency

The AC susceptibility (in-phase χ' and out-of-phase χ''), measured as a function of excitation frequency, for the FluidMAG-D sample from Chemicell GmbH is shown in Figure 3. Because the measurements were made on a liquid sample, both Brownian relaxation and Néel relaxation are important. The peak in χ'' at about 400 Hz is due to the Brownian relaxation and the gradual decrease in χ' and the nonzero value in χ'' at frequencies above about 10 kHz is due to the AC susceptibility contribution from the Néel relaxation. The experimental data were fitted to an AC susceptibility multicore particle model [*Öisjöen et al.*, 2010] as described earlier in section 2.1.2. Since this model is a superposition of both the Brownian and the Néel relaxation, the amount that each relaxation contributes to the total AC susceptibility at low frequencies can be determined. Brownian relaxation was estimated to be 72% of the total signal while Néel relaxation was 28%. A mean value of the magnetite nanocrystal size can be estimated from the Néel relaxation time determined from the used model for data fitting and using the Néel relaxation time expression (assuming low fields and negligible magnetic interactions):

$$\tau = \tau_0 \exp(K_a V / kT) \quad (1)$$

where τ is the Néel relaxation time; τ_0 is the attempt time, K_a is the magnetic anisotropy constant, V is volume, k is Boltzmann's constant, and T is temperature. From the data fitting, we get, $\tau = 1.2 \times 10^{-6}$ s; and

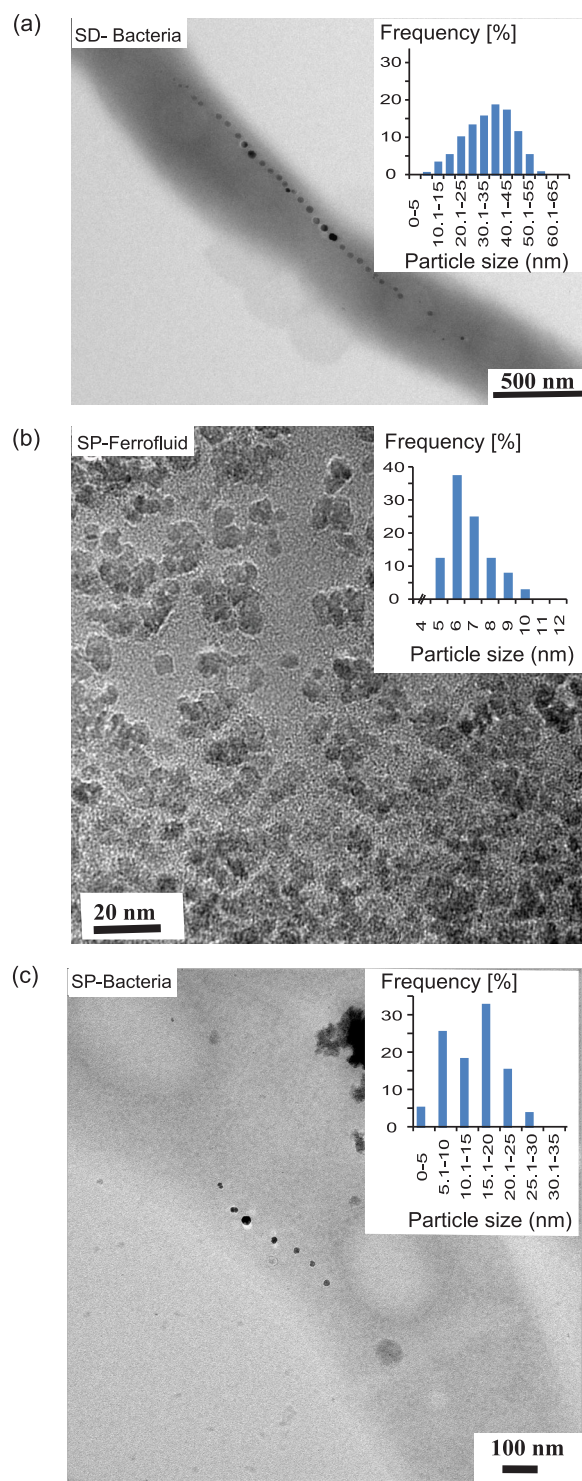


Figure 1. Bright-field transmission electron microscopic images of: (a) SD-bacteria, (b) SP-ferrofluid, and (c) SP-bacteria. Inset shows the corresponding particle size distributions as measured from TEM micrographs.

tion and the cross-sectional coercivity spectrum for the initial sample (0% SP-ferrofluid), an intermediate member of the series (64% SP-ferrofluid), and the final sample in the mixing series (94.2% of ferrofluid). It clearly demonstrates; (1) a shift in the peak FORC distribution function toward the origin of the FORC diagram, (2) an increase in the reversible peak of the induced magnetization, with a

assuming $K_a = 2 \times 10^4 - 4 \times 10^4 \text{ J/m}^3$ and $\tau_o = 10^{-9} - 10^{-10} \text{ s}$ (typical values of K_a and τ_o for magnetite nanocrystals at room temperature), the average value of the magnetite nanocrystal diameter is in the range of 11–15 nm for a spherical volume.

3.3. SD-SP Mixing Series

3.3.1. Mixture of SD-Bacteria and SP-Ferrofluid

M_{RS} , which is obtained from the hysteresis or FORC measurements, can be used to control whether remanent magnetization changed with the incremental addition of the SP sample. The value stays relatively constant with the incremental addition of SP ferrofluid, which demonstrates that the properties of the SD end-member are not changing during the addition of the SP component (Figure S1a). The difference between the values of H_{CR} obtained from the FORC and dc-IRM measurements reflects the different modes of magnetic field control between the two measurement methods, and the smaller measurement interval used in the FORC measurement. This difference becomes important with increasing content of SP material (Figure S1b). Hence the magnetic parameters, i.e., M_S , M_{RS} , H_C , and H_{CR} , for both SD-SP mixing series were obtained from the FORC measurements. The values of M_{RS} and H_{CR} have a standard deviation of $\pm 0.36 \mu\text{Am}^2$ and $\pm 0.37 \text{ mT}$ about their mean values, respectively. The standard deviation is well within the error estimation limit, which is $1.5 \mu\text{Am}^2$ for M_{RS} and 2 mT for H_{CR} . No systematic variation is observed in either parameter.

Figure 4a shows the magnetization and coercivity ratios on a Day plot obtained for a series of mixtures of SD-bacteria and SP-ferrofluid, as a function of increasing concentration of the SP fraction. Similar to the result of Dunlop and Carter-Stiglitz [2006], the values lie to the left of the theoretical curve for 10 nm. Our results show a good agreement, however, for a mixing line with 6 nm up to 54.7% addition by volume of ferrofluid. Above this, the remanence ratio is higher than expected, and this deviation increases with increasing concentration. Figures 5a, 5c, and 5e show the FORC distribution and the cross-sectional coercivity spectrum for the initial sample (0% SP-ferrofluid), an intermediate member of the series (64% SP-ferrofluid), and the final sample in the mixing series (94.2% of ferrofluid). It clearly demonstrates; (1) a shift in the peak FORC distribution function toward the origin of the FORC diagram, (2) an increase in the reversible peak of the induced magnetization, with a

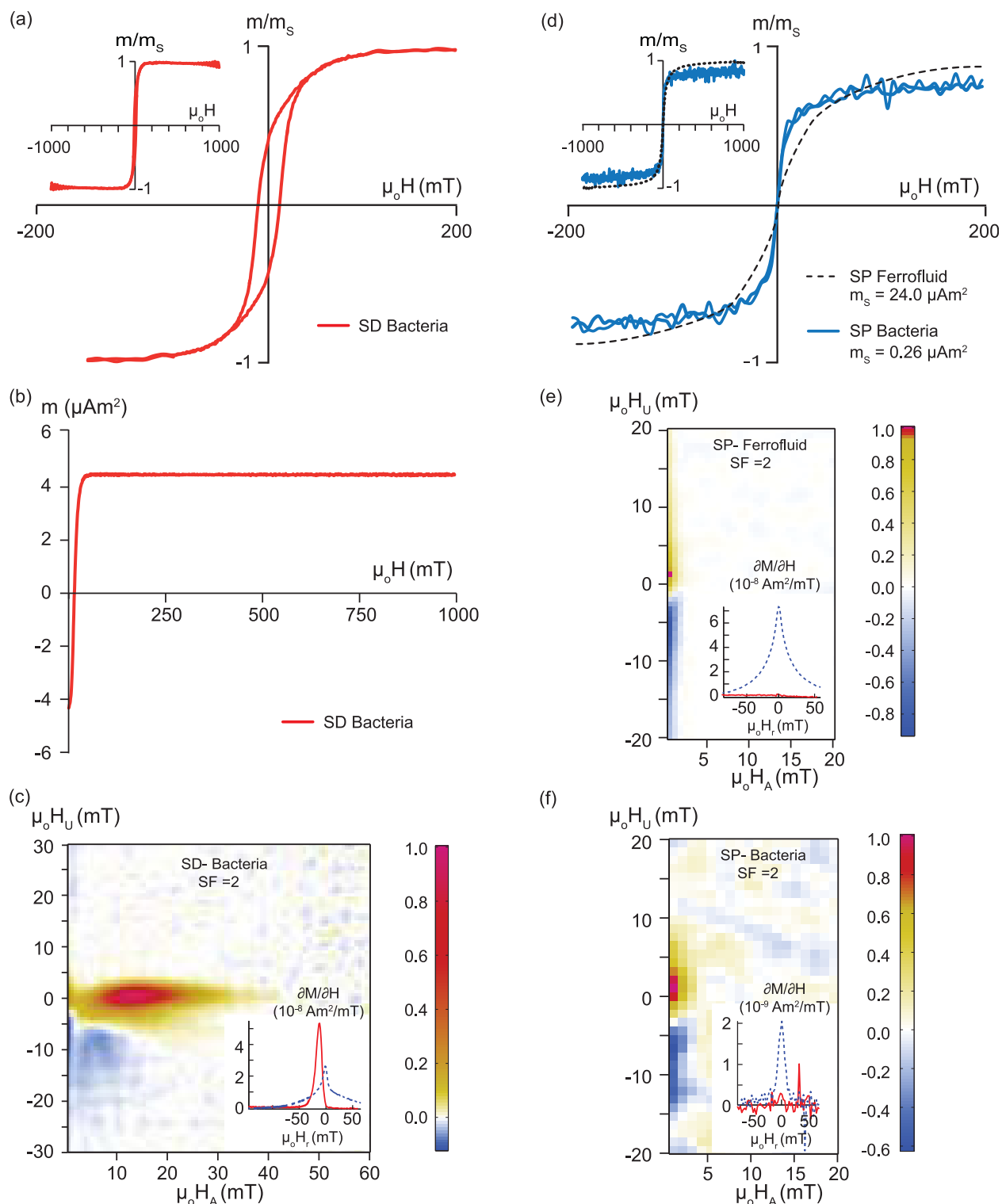


Figure 2. (a) Hysteresis loops, (b) dc-IRM, and (c) FORC distribution with an inset showing reversible and irreversible magnetization, for SD-bacteria. Note: $m_s = 10 \mu\text{A m}^2$ for SD-bacteria; (d) Hysteresis loops for SP samples; and FORC distributions with an inset showing reversible and irreversible magnetization, for (b) SP-ferrofluid and (c) SP- bacteria.

constant magnitude of the irreversible component, and (3) a constant magnitude of $H_{A1/2}$ of the high coercivity (SD) (Table S2) with incremental addition of SP sample to the SD-bacteria (Figures 5b, 5d, and 5f).

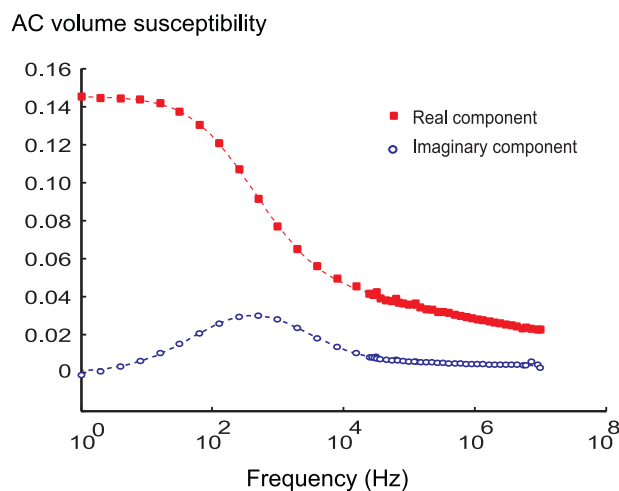


Figure 3. χ' and χ'' components of the AC susceptibility as a function of frequency at room temperature. Dotted lines show the fit to the AC susceptibility model.

magnetization (insets from Figures 6a, 6c, and 6e), and (3) an enhanced peak near the origin but a constant $H_{A1/2}$ for high-coercive phase at ≈ 14 mT as a function of incremental addition of SP-bacteria to the SD-bacteria (Figures 6b, 6d, and 6f).

4. Discussion

4.1. Role of Magnetic Interactions

The mixing series of SD bacteria with SP ferrofluid shows a good agreement with the theoretical mixing assuming particles with 6 nm diameter at low concentration but a deviation occurs with higher ferrofluid concentration. The curvature in the mixing line has also been seen by *Dunlop and Carter-Stiglitz* [2006], who attributed the sigmoidal shape to a change that occurs in the shape of the magnetization curve when the SP concentration exceeds 50%. A 6 nm particle size agrees with what was found on TEM images from the few isolated particles, but does not agree with the bulk magnetic behavior, for which the AC susceptibility suggests particles with 11–15 nm diameter. Aggregation of smaller particles could account for the difference. *Dormann et al.* [1999] also observed the effect of interparticle interaction in ferrofluids with higher concentration.

The mixing series of SD bacteria and SP bacteria follow a trend that lies below the theoretical mixing line for ~ 14 nm particles on the Day-Dunlop plot. The observed discrepancy could be accounted for by smaller SP particle size, which does not appear to be likely, or may be due to the presence of magnetic interaction, a skewed SP particle size or shape distribution, chemical purity of the samples, or a combination of these. In the following, we perform a set of experiments to test these different hypotheses for the observed discrepancy in the two sets of data.

$H_{A1/2}$, for the SD (large coercivity) and SP (low coercivity) are relatively constant with a standard deviation = ± 0.38 and 0.34 mT, and no systematic variations, again as expected from the hysteresis parameter. This suggests that SD-bacteria are essentially not influenced by the concentration of the SP-ferrofluid upon addition (Table T1). Similar is the case for SD-bacteria plus SP-bacteria mixing series except that in this case $H_{A1/2}$, for the large coercivity exhibits a larger standard deviation of ± 0.75 probably due to the low signal-to-noise ratio. The low-coercivity phase, however, has $H_{A1/2}$, relatively constant with a standard deviation of 0.06 mT.

We also apply a test, proposed by *Stacey and Banerjee* [1974], for examining the stability of the mixing series at each step. Their test suggests that for concentrations $> 54.7\%$, the SP-ferrofluid mixing series is unstable. For the SD-bacteria plus SP-bacteria mixing series, however, all measurements, except the last in the series, are stable.

3.3.2. Mixtures of SD-Bacteria and SP-Bacteria

The magnetization and coercivity ratios for the mixing series of SD-bacteria and SP-bacteria also fall below the theoretical mixing curve for SP grain size ≥ 14 nm on the Day-Dunlop plot (Figure 4b). Due to its weak magnetic signal, larger amounts of the SP bacteria had to be added to the sample, which gave a larger sample volume. For this reason, the last experimental point in this series no longer approximates a dipole signal. Similar to the ferrofluid mixing series, we also observe: (1) a shift in the peak FORC distribution function toward the origin of the FORC diagram (Figures 6a, 6c, and 6e), (2) an increase in the magnitude of the reversible peak and constant magnitude of irreversible peak of the induced

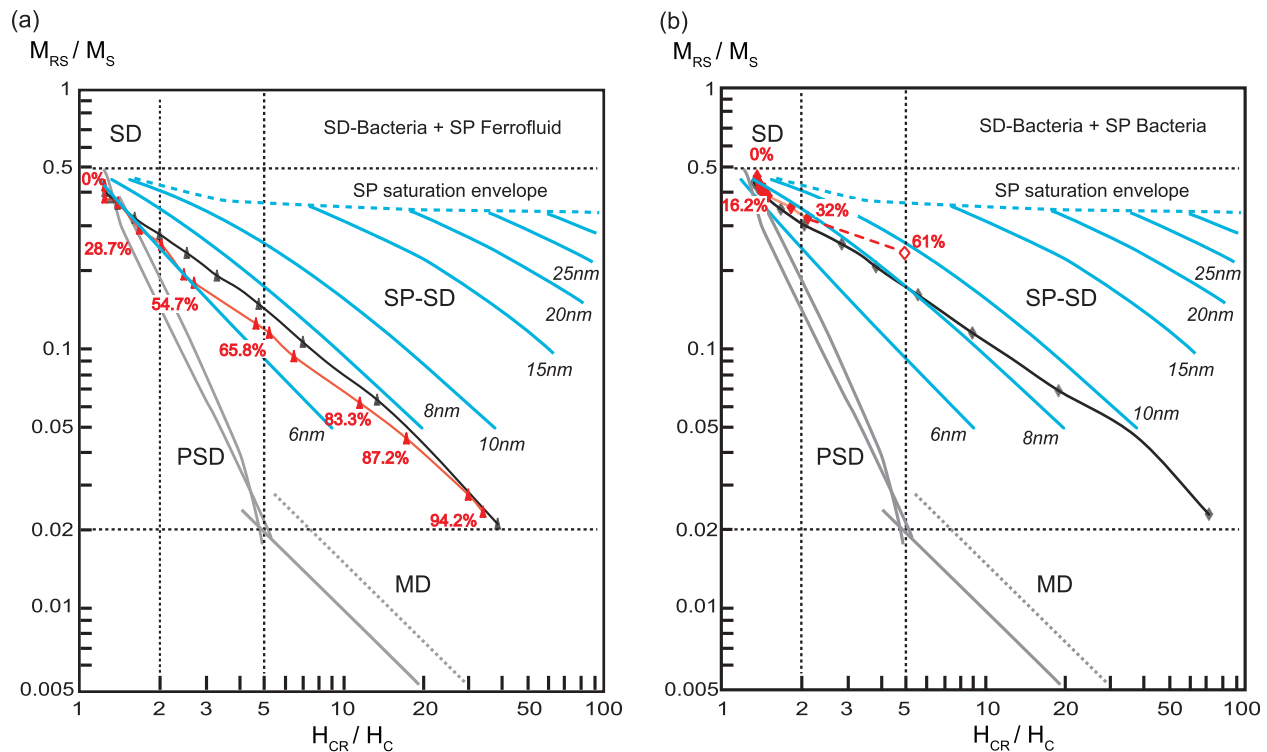


Figure 4. Day-Dunlop plot for mixtures of (a) SD-bacteria plus SP-ferrofluid and (b) SD-bacteria plus SP-bacteria. Red curve with solid points represents experimental data, while black curve with solid points are theoretically predicted mixing curves derived from the respective end members. Note: triangles are for mixing series with SP-ferrofluid, and diamonds for mixing series with SP-bacteria. Open diamond represents the measurements from nondipolar sample volume, and hence the dotted line is connecting this measurement point. Blue curves are the mixing curves of SD plus SP mixtures for different concentrations of SP content. Mixing lines for SD and PSD, and SD and MD are shown in grey. Concentration of the SP particles for the points on the mixing lines can be found in Table S1.

4.2. Remanent Magnetization Curves

We first test for interaction in the SD bacteria end-member by using R-value of the Wohlfarth-Cisowski test [Cisowski, 1981]. In an ideal case of noninteracting SD particles, the IRM acquisition and AF-demagnetization of IRM curves are symmetric with respect to each other, and their crossing point, R, is at 0.5. Figure S2 shows the results for the SD bacteria end-member, which has $R = 0.45$. This indicates that the SD-bacteria have negligible or no interactions. The small fraction of SP particles at the ends of chains would be enough to depress R slightly [Li et al., 2012].

4.3. AC Susceptibility Versus Temperature

Magnetic interaction in the SP end-members was assessed using AC susceptibility as a function of temperature. The AC susceptibility separated into its in-phase (χ') and out-of-phase (χ'') parts is shown in Figure 7. Both end-members show a broad blocking temperature spectrum that covers practically the entire temperature range.

Néel [1949] demonstrated that in the case of a broad distribution in blocking temperature, the χ'' component of AC susceptibility is proportional to the frequency dependence of the χ' susceptibility. This relationship can be used to verify the origin of thermal relaxation, and has been named the $\frac{\pi}{2}$ law (equation (2)) [Egli, 2009; Hrouda et al., 2013]:

$$\chi'' = -\frac{\pi}{2} \frac{\chi'(L) - \chi'(H)}{\ln(f(L) - f(H))} \quad (2)$$

where $\chi'(L)$ is the in-phase susceptibility at low frequency, $\chi'(H)$ is the in-phase susceptibility at high frequency, $f(L)$ and $f(H)$ are the low and high frequencies, respectively. The $\frac{\pi}{2}$ law was tested at frequencies $f(H) = 10,000$ Hz and $f(L) = 100$ Hz. The blocking behavior of a fraction of the SP-ferrofluid follows the $\frac{\pi}{2}$ law, but is violated at lower temperature (Figure 7b). Therefore, another phenomenon is responsible for χ''

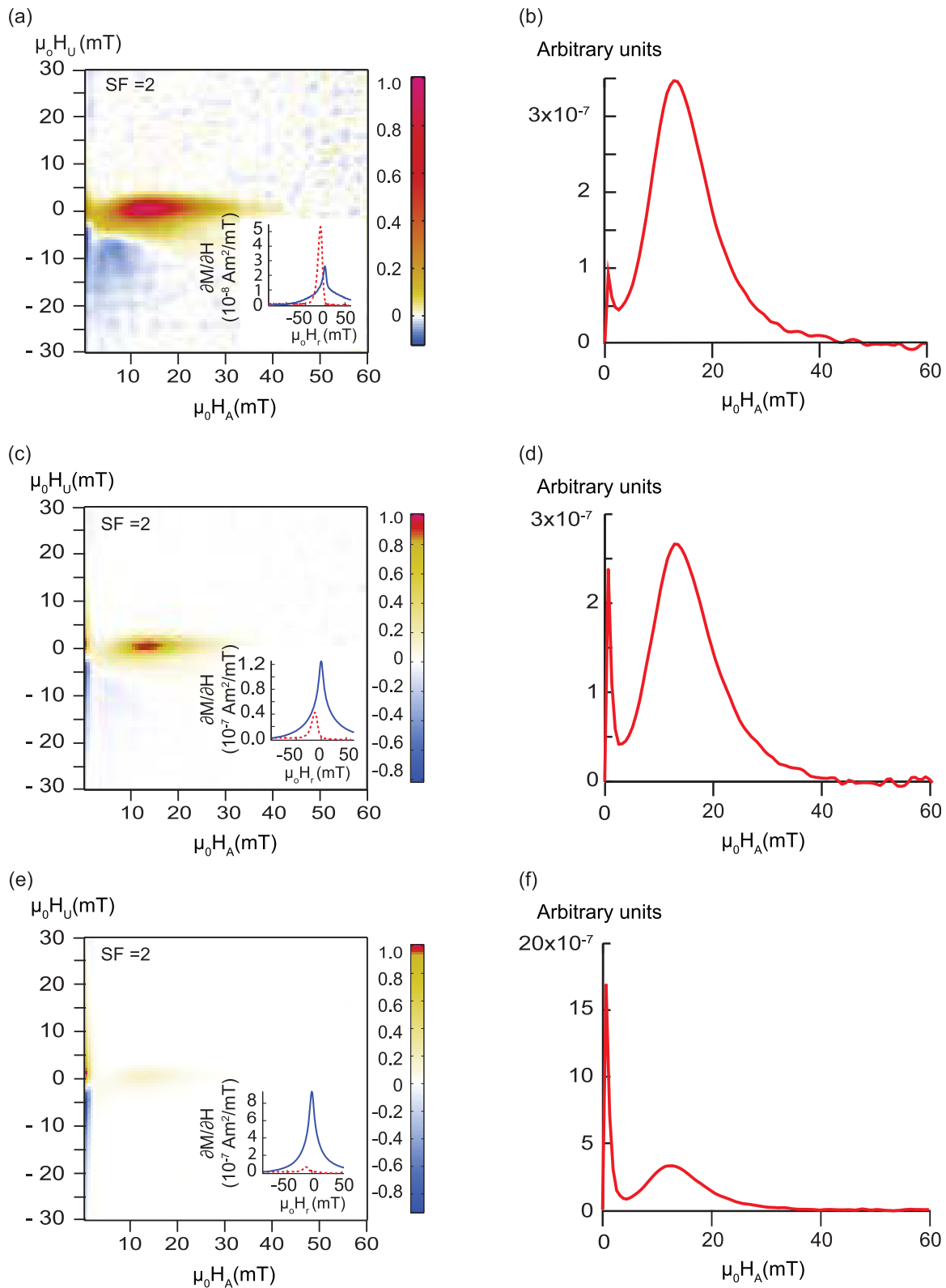


Figure 5. (left column) FORC distribution with an inset showing reversible and irreversible magnetization, and (right column) coercivity distribution taken at $\mu_0 H_U = 0$; (a and b) (100%) SD-bacteria end-member, (c and d) SD-bacteria plus 64% SP-ferrofluid mixture, and (e and f) SD-bacteria + 94.2% SP-ferrofluid mixture. The cross-sectional coercivity distribution is obtained by a profile along the horizontal axis H_A , through the FORC distribution function.

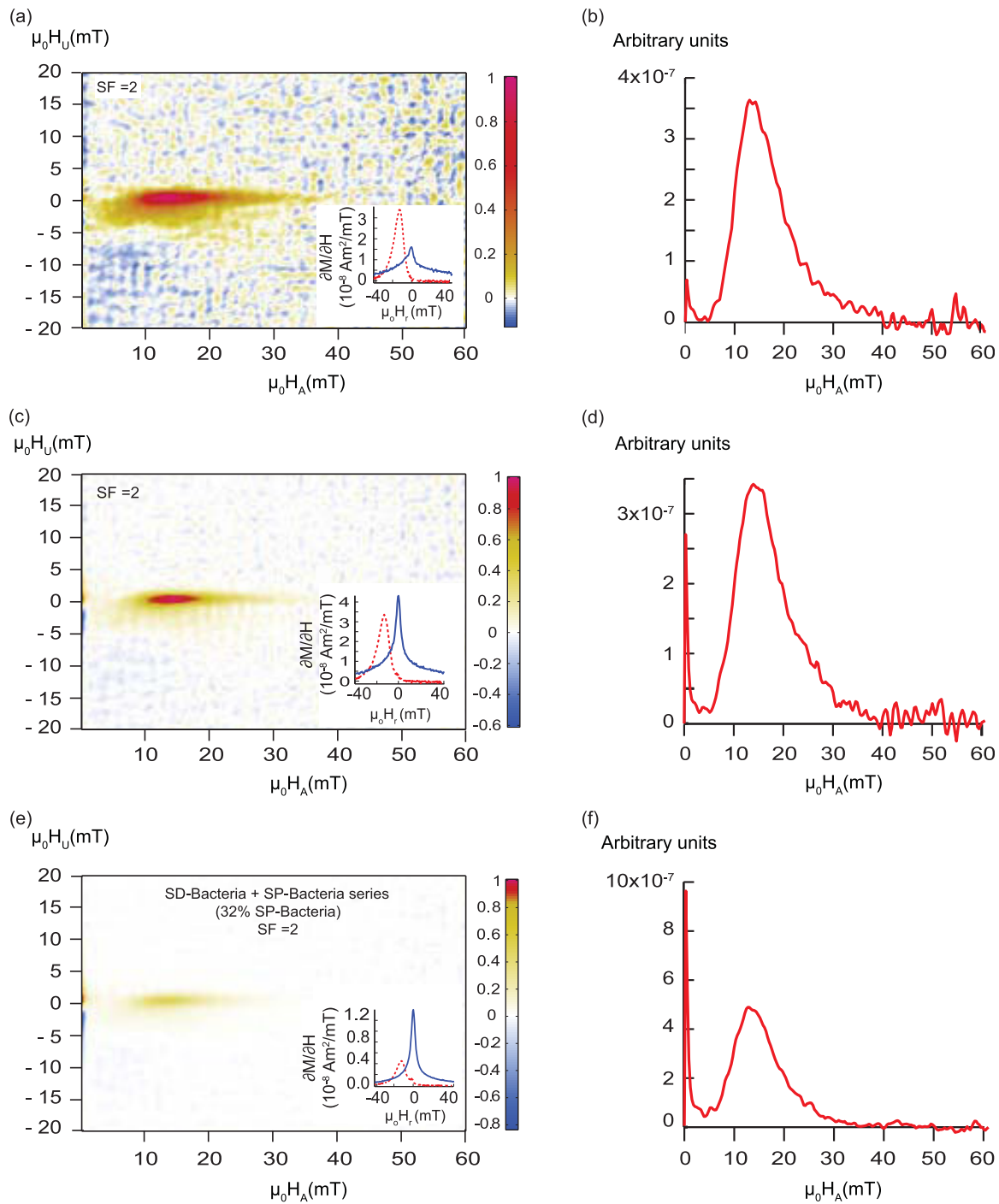


Figure 6. (left column) FORC distribution with an inset showing reversible and irreversible magnetization, and (right column) coercivity distribution taken at $\mu_0 H_u = 0$; (a and b) SD-bacteria end-member, (c and d) SD-bacteria plus 25.4% SP-bacteria mixture, and (e and f) SD-bacteria plus 32% SP-ferrofluid mixture.

below ~ 100 K. SP-bacteria, on the other hand, display a good agreement with the $\frac{\pi}{2}$ law (Figure 7d), which indicates that χ'' is purely due to thermally activated noninteracting SP grains [Shcherbakov and Fabian, 2005; Worm and Jackson, 1999].

The temperature, at which χ'' has a peak value, i.e., the average blocking temperature (T_B) of the particle system, can also be examined as a function of frequency. Because χ'' is comparatively unresponsive to temperature-related phenomena that are not associated with SP behavior, the change in T_B should follow

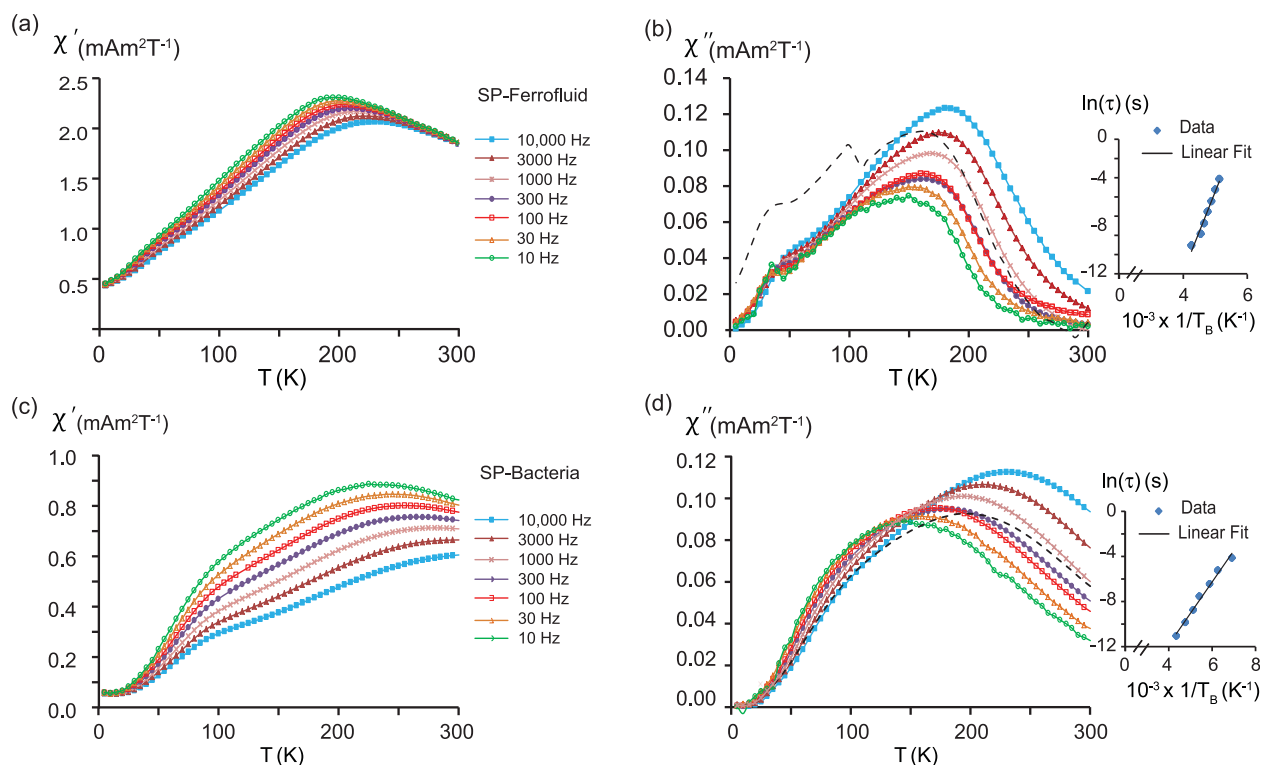


Figure 7. AC susceptibility as a function of temperature for SP-ferrofluid, (a) in-phase, (b) out of phase; and for SP-bacteria, (c) in-phase and (d) out of phase. Insets to Figures 7b and 7d show corresponding logarithm of relaxation time versus inverse of blocking temperature as a function of frequency. Note: dashed black curve is obtained using equation (2) for frequencies 10,000 and 100 Hz.

Néel-Brown theory (equation (1)). We observe that T_B increases with increasing frequency in both samples (Figure 7), and this relationship is shown in the insets to Figure 7 for both the SP-samples. The linear fit of the data gives τ_o , which should range between 10^{-8} and 10^{-11} s for a noninteracting SP assembly [Dormann *et al.*, 1999; Ghasemi, 2012]. The τ_o is 3.2×10^{-21} s for the SP-ferrofluid, which has no physical meaning because it is a few orders of magnitude below the empirically defined range. This suggests that equation (1) is inappropriate to describe the system of ferrofluid, and the inconsistency can be explained by moderate interactions among the magnetite particles in ferrofluid [Muxworthy, 2001]. In the case of SP-bacteria, τ_o is 1.1×10^{-10} s, which is well within the empirically accepted range, thereby further supporting the presence of noninteracting magnetite particles.

4.4. Determination of Mean Particle Size and Size Distribution Using Langevin Theory

The Langevin function can be applied to magnetization curves of the SP samples to estimate the mean effective magnetic particle size and their size distribution by approximating that magnetic interaction and magnetic anisotropy effects have negligible influence on the magnetization. Assuming a lognormal distribution of particle size, we model initial magnetization curves to compare the effective magnetic size with the physical size as depicted from TEM analysis. The simulated curves for initial magnetization are in good agreement with that obtained using experimental data for SP-ferrofluid (Figure 8a) and the SP-bacteria (Figure 8b). The SP-ferrofluid has a calculated average core diameter of 11.7 ± 1.5 nm (inset to Figure 8a). This value is close to the value provided by the manufacturer but also the average size obtained from the model fitting of the AC susceptibility data over the frequency range of 1 Hz–10 MHz. Therefore, measurements on the bulk ferrofluid sample suggest that the effective particle size is larger than what was determined from isolated particles in TEM analysis. SP-bacteria have a calculated mean diameter of 13.4 ± 1.5 nm and agree with the TEM analysis (inset to Figure 8b). The magnetosomes of SP-bacteria of this mutant strain are likely to follow a normal size distribution. The SP-bacteria used in this study, however, showed a closer fit by

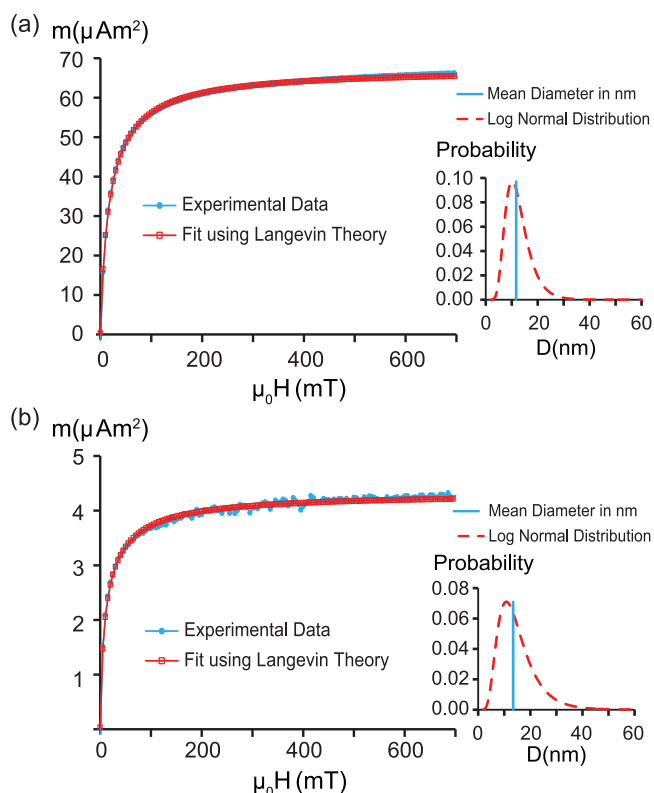


Figure 8. Initial magnetization as a function of applied field at room temperature for: (a) SP-ferrofluid and (b) SP-bacteria. Solid circles represent the experimental data points, and open squares are from simulation using Langevin theory applied to SP state. Corresponding insets show the probability as a function of particle diameter.

mixtures. It corresponds to a balance point field, and was determined from the magnetization curves of the end-members of the two series. For SD-bacteria, we use the magnetization curve between $M = -M_{RS}$ and $H = H_C$, and for the two SP samples, we use the initial magnetization to obtain a balance point field corresponding to different volume fraction of the SD component. The balance point field is defined as the field at which the magnetization of the SD component is equal in magnitude, but in opposite direction, with respect to the magnetization of the SP component. Experimental and theoretical data for the mixing series of SD-bacteria and SP-ferrofluid show a good agreement for low SP concentrations and again for the final samples (Figure 4a). There is a departure when the SP concentrations are 60% or higher, this could be explained by interactions within the SP-ferrofluid, as suggested by various magnetic methods described above. Therefore at low concentrations, there may be less interaction between the SP particles, but this increases with higher concentrations. This would cause a deviation to higher coercivity ratios. It should be noted, however, that even the sample with the highest SP-ferrofluid concentration lies below the theoretical 10 nm curve on the Day-Dunlop plot. Figure 4b displays experimental data and the theoretical fit for the mixtures of SD-bacteria and SP-bacteria. The experimental data match theoretical prediction trends based on the end-members. It is important to note, however, that the curve lies below what one would expect for 14 nm SP particles.

5. Conclusions

Both experimental and theoretically predicted data of the two SD-SP mixing series show inconsistency with the SD-SP curves on the Day plot as predicted by Dunlop [2002a] for their respective grain sizes. The mixtures of SD-bacteria with SP-ferrofluids follow the predicted mixing trends on the Day-Dunlop plot up to 54.7% addition of ferrofluid by volume assuming the TEM defined particle size of 6 nm. AC-susceptibility and initial magnetization curves suggest moderate magnetic interactions in the ferrofluid. Modeling of

assuming a lognormal distribution of particle sizes. Assuming either a normal size distribution or lognormal size distribution does not produce a significant difference in the mean size estimation.

4.5. Theoretical Determination of Mixing Series Using End-Members

An alternative approach to compare experimental results with the theoretical curves of Dunlop [2002a] is to assume a linear mixing model based on the magnetic properties of the end-members. This approach uses the following equations to evaluate magnetization and coercivity ratios for mixtures:

$$\frac{M_{RS}}{M_S} = f_{SD} \left(\frac{M_{RS}}{M_S} \right)_{SD} \quad (3)$$

where, f_{SD} corresponds to the volume fraction of SD, and $\left(\frac{M_{RS}}{M_S} \right)_{SD} = 0.46$ for SD-bacteria and

$$\frac{H_{CR}}{H_C} = \frac{(H_{CR})_{SD}}{(H_C)_{f_{SD}}} \quad (4)$$

with, $(H_{CR})_{SD} = 14.2$ mT, the remanent coercivity for the SD-bacteria.

H_C represents the coercivity of the

Langevin behavior and the Néel behavior in an AC susceptibility model applied to experimental data indicates a larger particle core size (≈ 11 nm), which may reflect the size of aggregates produced from magnetic interactions or agglomeration of smaller grains. Therefore, the aggregated particles are still SP, but their core diameter increase. This leads to a deviation of the mixing curve toward larger particle size.

The experimental mixing line for the mixtures of SD-bacteria and SP-ferrofluid follows the theoretically predicted line, but suggests lower coercivity and magnetization ratios than what would be expected from the mixing lines of Dunlop [2002a]. In both series, adjustment of particle size and shape distribution in the theory may bring experimental results closer to the theoretical SD-SP mixing lines of Dunlop [2002a].

However, these results demonstrate that caution should be used when trying to determine the percentage of SP particles and their size from the SD-SP mixing curves on Day-Dunlop plots. Such mixtures may lie in the PSD field on the plot and be indistinguishable from mixtures of SD and PSD grains or SD and MD grains. Tests for SP contributions in a rock or sediments would help eliminate this as an option when interpreting hysteresis data on the Day-Dunlop plot. Therefore, without any corroborative information, a simple comparison of magnetization and coercivity ratios with mixing curves on the Day-Dunlop plot may lead to an ambiguous interpretation of particle size.

Acknowledgments

We thank H.-P. Hächler from the Laboratory of Natural Magnetism at ETH Zurich for the preparation of sample holders and technical support during the measurements, and S. Handschin from ScopeM at ETH-Zurich for performing TEM micrographs of SD-bacteria. We thank L. Lanci for helpful discussions, and W. Lowrie is acknowledged for thoughtful discussion and reading the manuscript. We thank K. Fabian, M. Jackson, and M. Dekkers for their thorough and thoughtful reviews. This work was supported by The European Union (Project Bio2MaN4MRI n 245542). The work on the AC susceptibility versus frequency analysis (Acreo) in this study is financed from the EU FP7 NMP project NanoMag grant agreement 604448. Data to support the main findings of this article are available in supporting information Tables S1 and S2, and other data can be made available upon request to the corresponding author.

References

- Carter-Stiglitz, B., B. Moskowitz, and M. Jackson (2001), Unmixing magnetic assemblages and the magnetic behavior of bimodal mixtures, *J. Geophys. Res.*, *106*(B11), 26,397–26,411.
- Carvalho, C., A. R. Muxworthy, and D. J. Dunlop (2006), First-order reversal curve (FORC) diagrams of magnetic mixtures: Micromagnetic models and measurements, *Phys. Earth Planet. Inter.*, *154*(3–4), 308–322.
- Cinku, M. C., Z. M. Hisarli, N. Orbay, T. Ustaomer, A. M. Hirt, S. Kravchenko, O. Rusakov, and N. Sayin (2013), Evidence of early cretaceous remagnetization in the Crimean peninsula: A palaeomagnetic study from mesozoic rocks in the Crimean and western pontides, conjugate margins of the western Black Sea, *Geophys. J. Int.*, *195*(2), 821–843.
- Cisowski, S. (1981), Interacting vs non-interacting single domain behavior in natural and synthetic samples, *Phys. Earth Planet. Inter.*, *26*(1–2), 56–62.
- Day, R., M. Fuller, and V. A. Schmidt (1977), Hysteresis properties of titanomagnetites—Grain-size and compositional dependence, *Phys. Earth Planet. Inter.*, *13*(4), 260–267.
- Denham, C. R., R. P. Blakemore, and R. B. Frankel (1980), Bulk magnetic-properties of magnetotactic bacteria, *IEEE Trans. Magn.*, *16*(5), 1006–1007.
- Di Chiara, A., L. Tauxe, and F. Speranza (2014), Paleointensity determination from São Miguel (Azores Archipelago) over the last 3ka, *Phys. Earth Planet. Inter.*, *234*, 1–13.
- Dormann, J. L., D. Fiorani, and E. Tronc (1999), On the models for interparticle interactions in nanoparticle assemblies: Comparison with experimental results, *J. Magn. Mater.*, *202*(1), 251–267.
- Dunlop, D. J. (2002a), Theory and application of the Day plot (Mrs/Ms versus Hcr/Hc): 1. Theoretical curves and tests using titanomagnetite data, *J. Geophys. Res.*, *107*(B3), 2056, doi:10.1029/2001JB000486.
- Dunlop, D. J. (2002b), Theory and application of the Day plot (Mrs/Ms versus Hcr/Hc): 2. Application to data for rocks, sediments, and soils, *J. Geophys. Res.*, *107*(B3), 2057, doi:10.1029/2001JB000487.
- Dunlop, D. J., and B. Carter-Stiglitz (2006), Day plots of mixtures of superparamagnetic, single-domain, pseudosingle-domain, and multidomain magnetites, *J. Geophys. Res.*, *111*, B12S09, doi:10.1029/2006JB004499.
- Egli, R. (2009), Magnetic susceptibility measurements as a function of temperature and frequency. I: Inversion theory, *Geophys. J. Int.*, *177*(2), 395–420.
- Ferguson, R. M., A. P. Khandhar, C. Jonasson, J. Blomgren, C. Johansson, and K. M. Krishnan (2013), Size-dependent relaxation properties of monodisperse magnetite nanoparticles measured over seven decades of frequency by ac susceptometry, *IEEE Trans. Mag.*, *49*(7), 3441–3444.
- Fischer, H., G. Mastrogiacomo, J. F. Löffler, R. J. Warthmann, P. G. Weidler, and A. U. Gehring (2008), Ferromagnetic resonance and magnetic characteristics of intact magnetosome chains in *Magnetospirillum gryphiswaldense*, *Earth Planet. Sci. Lett.*, *270*(3–4), 200–208.
- Ghasemi, A. (2012), Magnetic properties of substituted strontium ferrite nanoparticles and thin films, *J. Magn. Mater.*, *324*(7), 1375–1380.
- Guzmán, O., V. Costanzo-Álvarez, M. Aldana, and M. Díaz (2011), Study of magnetic contrasts applied to hydrocarbon exploration in the Maturín Sub-Basin (eastern Venezuela), *Stud. Geophys. Geod.*, *55*(2), 359–376.
- Hao, Q., F. Oldfield, J. Bloemendal, and Z. Guo (2012), Hysteresis and thermomagnetic properties of particle-sized fractions from loess and palaeosol samples spanning 22 Myr of accumulation on the Chinese loess plateau, *Geophys. J. Int.*, *191*(1), 64–77.
- Heslop, D., and A. P. Roberts (2012), A method for unmixing magnetic hysteresis loops, *J. Geophys. Res.*, *117*, B03103, doi:10.1029/2011JB008859.
- Hrouda, F., J. Pokorný, J. Jezek, and M. Chadima (2013), Out-of-phase magnetic susceptibility of rocks and soils: A rapid tool for magnetic granulometry, *Geophys. J. Int.*, *194*(1), 170–181.
- Jackson, M., H.-U. Worm, and S. K. Banerjee (1990), Fourier analysis of digital hysteresis data: rock magnetic applications, *Phys. Earth Planet. Inter.*, *65*(1–2), 78–87.
- Kapper, K. L., F. Donadini, M. Mauvilly, S. Panovska, and A. M. Hirt (2014), New directional archeomagnetic data of burned cave sediments from Switzerland and geomagnetic field variations in Central Europe, *Geophys. J. Int.*, *198*(2), 1208–1221.
- Krishnan, K. M. (2010), Biomedical nanomagnetism: A spin through possibilities in imaging, diagnostics, and therapy, *IEEE Trans. Magn.*, *46*(7), 2523–2558.
- Kumari, M., M. Widdrat, É. Tompa, R. Uebe, D. Schüler, M. Pósfai, D. Faivre, and A. M. Hirt (2014), Distinguishing magnetic particle size of iron oxide nanoparticles with first-order reversal curves, *J. Appl. Phys.*, *116*(12), 124304.

- Lanci, L., and D. V. Kent (2003), Introduction of thermal activation in forward modeling of hysteresis loops for single-domain magnetic particles and implications for the interpretation of the Day diagram, *J. Geophys. Res.*, *108*(B3), 2142, doi:10.1029/2001JB000944.
- Lees, J. A. (1997), Mineral magnetic properties of mixtures of environmental and synthetic materials: Linear additivity and interaction effects, *Geophys. J. Int.*, *131*(2), 335–346.
- Li, G., S. Sizaret, Y. Branquet, L. Barbanson, Y. Chen, B. Wang, C. Wu, L. Gu, and L. Shu (2014), Initial geometry and paleoflow reconstruction of the Yamansu skarn-related iron deposit of eastern Tianshan (China) from paleomagnetic and magnetic fabrics investigations, *J. Asian Earth Sci.*, *93*, 1–14.
- Li, J., W. Wu, Q. Liu, and Y. Pan (2012), Magnetic anisotropy, magnetostatic interactions and identification of magnetofossils, *Geochem. Geophys. Geosyst.*, *13*, Q10Z51, doi:10.1029/2012GC004384.
- Lohsse, A., S. Ullrich, E. Katzmann, S. Borg, G. Wanner, M. Richter, B. Voigt, T. Schweder, and D. Schuler (2011), Functional analysis of the magnetosome island in *Magnetospirillum gryphiswaldense*: The mamAB operon is sufficient for magnetite biomineralization, *PLoS One*, *6*(10), e25561, doi:10.1371/journal.pone.0025561.
- Moskowitz, B. M., R. B. Frankel, and D. A. Bazylinski (1993), Rock magnetic criteria for the detection of biogenic magnetite, *Earth Planet. Sci. Lett.*, *120*(3–4), 283–300.
- Muxworthy, A. R. (2001), Effect of grain interactions on the frequency dependence of magnetic susceptibility, *Geophys. J. Int.*, *144*(2), 441–447.
- Muxworthy, A. R., D. Heslop, and W. Williams (2004), Influence of magnetostatic interactions on first-order-reversal-curve (FORC) diagrams: A micromagnetic approach, *Geophys. J. Int.*, *158*(3), 888–897.
- Ne, A. J. (2005), A high-precision model of first-order reversal curve (FORC) functions for single-domain ferromagnets with uniaxial anisotropy, *Geochem. Geophys. Geosyst.*, *6*, Q05010, doi:10.1029/2004GC00877.
- Néel, L. (1949), Influence des fluctuations thermiques sur l'aimantation de grains ferromagnétiques très fins, *Comptes rendus hebdomadaires des séances de l'Académie des Sciences (Paris), Sér. B*, *228*, 664–666.
- Öisjöen, F., J. F. Schneiderman, A. P. Astalan, A. Kalabukhov, C. Johansson, and D. Winkler (2010), A new approach for bioassays based on frequency- and time-domain measurements of magnetic nanoparticles, *Biosensors Bioelectr.*, *25*(5), 1008–1013.
- Pan, Y., N. Petersen, M. Winklhofer, A. F. Davila, Q. Liu, T. Frederichs, M. Hanzlik, and R. Zhu (2005), Rock magnetic properties of uncultured magnetotactic bacteria, *Earth Planet. Sci. Lett.*, *237*(3–4), 311–325.
- Pike, C. R., A. P. Roberts, and K. L. Verosub (1999), Characterizing interactions in fine magnetic particle systems using first order reversal curves, *J. Appl. Phys.*, *85*(9), 6660–6667.
- Pike, C. R., A. P. Roberts, and K. L. Verosub (2001), First order reversal curve diagrams and thermal relaxation effects in magnetic particles, *Geophys. J. Int.*, *145*(3), 721–730.
- Roberts, A. P., C. R. Pike, and K. L. Verosub (2000), First-order reversal curve diagrams: A new tool for characterizing the magnetic properties of natural samples, *J. Geophys. Res.*, *105*(B12), 28,461–28,475.
- Roberts, A. P., L. Chang, C. J. Rowan, C.-S. Horng, and F. Florindo (2011), Magnetic properties of sedimentary greigite (Fe₃S₄): An update, *Rev. Geophys.*, *49*, RG1002, doi:10.1029/2010RG000336.
- Shcherbakov, V. P., and K. Fabian (2005), On the determination of magnetic grain-size distributions of superparamagnetic particle ensembles using the frequency dependence of susceptibility at different temperatures, *Geophys. J. Int.*, *162*(3), 736–746.
- Stacey, F. D., S. K. Banerjee (1974), *The Physical Principles of Rock Magnetism*, Elsevier Sci. Publ., Amsterdam, 195 pp.
- Stanton, T., P. Riisager, M. F. Knudsen, and T. Thordarson (2011), New palaeointensity data from Holocene Icelandic lavas, *Phys. Earth Planet. Inter.*, *186*(1–2), 1–10.
- Tauxe, L., T. A. T. Mullender, and T. Pick (1996), Potbellies, wasp-waists, and superparamagnetism in magnetic hysteresis, *J. Geophys. Res.*, *101*(B1), 571–583.
- Tianshui, Y., L. I. Haiyan, W. U. Huaichun, Y. Zhenyu, Z. Shihong, and H. Masayuki (2012), Reliability of relative paleointensity recorded in Chinese loess–paleosol sediments, *Acta Geol. Sin.*, *86*(5), 1276–1288.
- von Dobeneck, T. (1996), A systematic analysis of natural magnetic mineral assemblages based on modelling hysteresis loops with coercivity-related hyperbolic basis functions, *Geophys. J. Int.*, *124*(3), 675–694.
- Winklhofer, M., and G. T. Zimanyi (2006), Extracting the intrinsic switching field distribution in perpendicular media: A comparative analysis, *J. Appl. Phys.*, *99*(8), 08E710.
- Worm, H.-U., and M. Jackson (1999), The superparamagnetism of Yucca Mountain Tuff, *J. Geophys. Res.*, *104*(B11), 25,415–25,425.